Veiga-López, Fernando; Martínez-Ruiz, Daniel; Kuznetsov, Mike; Sánchez-Sanz, Mario. (2020), Thermoacoustic analysis of lean premixed hydrogen flames in narrow vertical channels, *Fuel,* v. 278, 118212.

DOI: https://doi.org/10.1016/j.fuel.2020.118212

Thermoacoustic Analysis of Lean Premixed Hydrogen Flames in Narrow Vertical Channels

Fernando Veiga-López[a,*], Daniel Martínez-Ruiz[b], Mike Kuznetsov[c], Mario Sánchez-Sanz[a]

[a] *Departamento de Ingeniería Térmica y de Fluidos, Universidad Carlos III de Madrid, 28911, Leganés, Madrid, España.*
[b] *ETSIAE, Universidad Politécnica de Madrid, 28040, Madrid, España.*
[c] *Institut für Kern- un Energietechnick, Karlsruhe Institut für Technologie, 76344, Eggenstein-Leopoldshafen, Deutschland.*

Abstract

Thermoacoustic instabilities arise for lean hydrogen-air flames propagating in narrow channels. We provide here a detailed experimental analysis of such phenomena in a semi-confined vessel, analyzing the effect of the mixture composition, geometry and gravity on the onset of acoustic-driven flame vibrations.

Downward-propagating flames leaner than a critical value vibrate smoothly and transit to the secondary oscillating instability, which develops strong variations of pressure that couple with the propagation dynamics. The transition threshold changes during the propagation along very narrow channels, where heat losses are no longer negligible. The parametric region of equivalence ratio for the secondary thermoacoustic instability diminishes, showing an additional transition for very lean flames. There, the front breaks into

*fveiga@ing.uc3m.es

June 7, 2020

several structures and the flame-wave feedback becomes weaker.

The influence of gravity is studied by comparing upward and downward propagating flames, where the Rayleigh-Taylor instability arises for sufficiently small values of the Froude number in slow-propagating lean flames. For a constant mixtue, buoyancy-driven upward-propagating flames develop less wrinkled fronts than those propagating downwards, and remain unresponsive to acoustic-front interaction. We show here a direct relation between front shape and thermoacoustics.

In agreement with previous studies [1–3], curvature and strain effects on conduction and diffusion characterize the response of the flame to pressure perturbations, with the Markstein number controlling the aforementioned transition. Nevertheless, the theoretical analyses found in the literature can only be used on nearly equidiffusional mixtures, and are not accurate enough to describe the highly diffusive fuel mixtures (i.e. lean hydrogen-air flames) considered in our experiments.
Keywords: Hydrogen, narrow channels, Markstein number, thermoacoustic instabilities, gravity

---

1. Introduction

Hydrogen is one of the near-future green-fuel candidates for power generation systems due to its high energy density and CO_2-free emissions [4]. Although lean premixed burning rises as one of the most efficient combustion procedures, lean hydrogen flames are inherently unstable. The density

change across the front, the competition between heat and mass diffusion, the effect of gravity and the interaction between acoustic waves and the front have a strong effect on the outline and behavior of premixed flames [5, 6]

In particular, the vibratory motion of premixed flames first reported by Mallard and Le Chatelier [7] is studied here. The so-called thermoacoustic instabilities appear as a result of the coupling between reactive fronts and acoustic pressure waves in confined or semi-confined combustion chambers, which can potentially lead to critical failure of the system. Following the original Rayleigh's criterion, pressure waves are amplified –theoretically– if they are in phase with the unsteady heat release of the flame. This transfer of energy between the front and the acoustic waves competes with the different damping mechanisms that arise in real configurations, such as viscous layers or heat losses. The competition between various effects may lead to an amplification, thus yielding a destabilizing effect, or an attenuation of the acoustic waves. First experimental studies reporting the marked behavior of oscillating flames under smooth and violent regimes [8, 9], directly related it to acoustic coupling. Later, most experimental studies have investigated the behavior of premixed downward-propagating hydrocarbon flames in tubes [10–12], always moving towards the closed end of the chamber. Other geometries, such as a Taylor-Couette [13] and narrow-channel Hele-Shaw burners [1], were more recently investigated using methane, propane and dymethilether (DME) mixed with air. Also, lean hydrogen-air mixtures were tested in squared cross-section tubes [14], which considered the effect

of acoustic forcing. Two main regimes of the acoustic oscillatory flames are recurrently found by all these authors as a result of the aforementioned coupling mechanism: the primary instability, a smooth and unwrinkled front vibration; and the secondary instability (also self-excited parametric), violent pulses of the corrugated front.

The first theoretical explanations to thermoacoustic instabilities were given by Markstein under the context of SQUID project after World War II [15, 16], who proposed the parametric instability driven by an imposed acoustic oscillating flow that interacted with the flame [17]. These analyses led to the Mathieu's equation, which defined a stability criteria linking the amplitude and frequency of the oscillatory velocity and the wavelength of the perturbation. Later revisited by other authors [13, 18], the derived stability diagrams were found to be strongly affected by diffusive and curvature effects, thus controlled by the Markstein number $\mathscr{M}$. Although these studies aim to extract information on the stability of the flame response upon a forcing fixed acoustic field, the self-excited acoustic oscillations of the flame have been theoretically explored only recently [19, 20]. To the best of our knowledge, all theoretical efforts based on the interaction of the acoustic field and the reacting front agree with the definition of the controlling parameter $\mathscr{M}$ in near-equidiffusional mixtures with $Le \simeq 1$.

In favor of clarity and providing further understanding, experiments with highly-diffusive species, namely hydrogen-air mixtures, are therefore required. For this purpose, the selected burner configuration consists of a quasi-two-

dimensional Hele-Shaw cell, where the damping mechanisms can be adjusted and visual inspection can provide quantitative data. Preceding experiments in Hele-Shaw cells analyzed thermoacoustic instabilities for several hydrocarbons [1, 2], where the value of the Markstein number was found to be an important parameter playing a role in the different acoustic-flame interaction regimes. Although the effect of gravity was neglected by positioning the chamber horizontally, vertical channels are studied here with the reaction fronts propagating in favor and against gravity acceleration. This work further analyzes thermoacoustic instabilities and related physical processes for lean hydrogen-air premixed flames in a very narrow channel configuration. The importance of the equivalence ratio, the role of the channel thickness as well as the effect of gravity are reported here.

The paper is structured as follows. Section 2 describes the experimental setup and the procedure followed during the experimental campaign. Additionally, important parameters of the study cases are given here. Section 3 shows the main results obtained and detailed discussions of the main findings of the work. In particular, the effects of equivalence ratio, channel thickness and buoyancy forces on the propagation of the flames. Finally, conclusions found in this work are given in section 4.

2. Experimental Setup and Procedure

The combustion chamber used in the following experiments is conformed by two 10-mm-thick plexiglass plates separated by a PVC sealing hollow

frame as sketched in Fig. 1, being the total volume enclosed by the cell $950 \times 200 \times (10-4)$ mm^3 ($L \times W \times h$). The gap size (h) can be modified to assess effects related to heat losses and viscous damping. Also, the combustion chamber can be flipped vertically to study upward- or downward-propagating flames, thus reporting the importance of the Rayleigh-Taylor instability on modifying thermoacoustic dynamics.

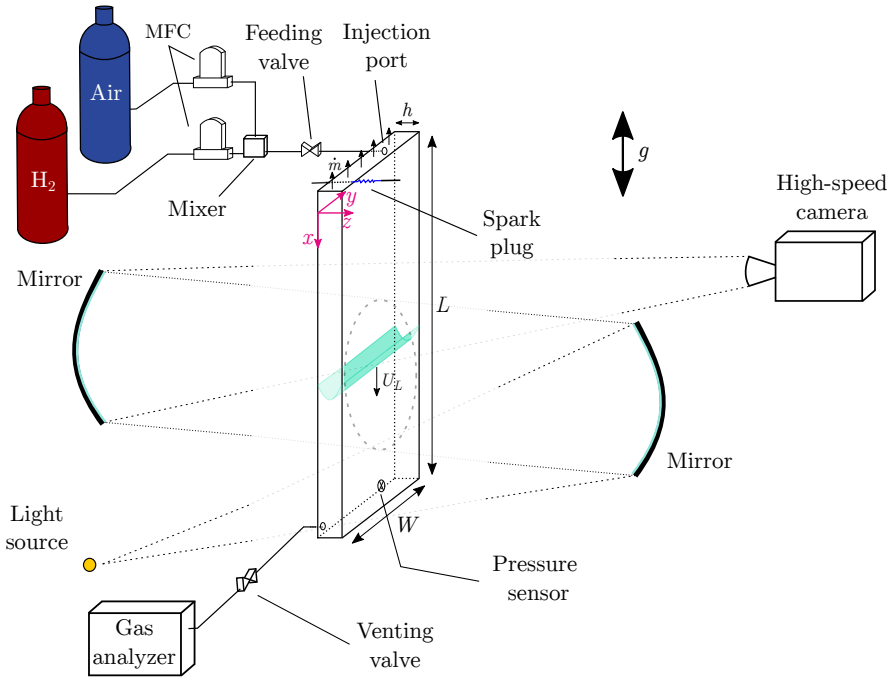

Figure 1: Schematic of the experimental setup. High-speed images recorded using a Z-shape Schlieren system. The dimensions of the cell $L \times W \times h$ are included in the sketch. The black arrows at the ignition end of the chamber represent the totally unobstructed exit of the hot reaction products.

Hydrogen and air are mixed before entering the combustion chamber, controlling the fuel-to-air ratio with two precise EL-FLOW mass-flow controllers, which keep the error of the concentration of hydrogen within $\pm 1\%$.

Prior to combustion, the mixture is fed via an injection port located at the ignition side of the chamber, keeping this end closed. The test mixture replaced the more dense air through an opening valve at the opposite side. The complete charge of the chamber is checked at the outlet line using a gas analyzer Rosemount^{TM} CT5400 by comparing the inlet and outlet mixture composition. After a minute of exposure, the ignition end is fully reopened, the opposite-end valve is closed, and the mixture is ignited by a spark plug. The flames propagate towards a completely closed end in all the cases studied here, which produces a necessary acoustic reflection to trigger the phenomena under study.

A Z-shape Schlieren optical system with a LED light source, two 280-mm-diameter mirrors, a set of lenses and a high-speed camera (Photron FASTCAM SA 1.1 shooting at 1000 fps) is used to capture images of the flame front propagation. Due to the limited size of the mirrors, only partial visualization of the setup was possible during each experiment. The chamber can be shifted vertically to change and capture the region under consideration, thus covering the whole channel length in consecutive trials. Additionally, a pressure sensor (PCB M113B12) is located at the far closed end $x = 900$ mm to measure the acoustic pressure oscillations, with an accuracy of $\pm 0.8\%$.

The main properties of the analyzed mixtures are shown in Table 1 and they were calculated following the methodology introduced by Yañez and Kuznetsov [14]. Here ϕ indicates the equivalence ratio of the mixture calculated as $([H_2]/[O_2])/(H_2]/[O_2])_{st}$ where $[X]$ represents the percentage in

%vol. H_2	ϕ	T_b [K]	S_L [cm/s]	Le	δ_T [mm]	Fr^2 $\times 10^{-3}$
6	0.15	784	2.9	0.32	0.83	9
6.5	0.17	823	3.6	0.33	0.67	13
9.5	0.25	1055	10	0.34	0.24	102
10	0.26	1093	11	0.34	0.22	123
11	0.29	1169	15	0.34	0.16	229
12	0.32	1244	19	0.35	0.13	368
13	0.36	1319	23	0.35	0.10	539
14	0.39	1393	28	0.36	0.09	799
15	0.42	1466	35	0.36	0.07	1249

Table 1: Properties of lean hydrogen-air mixtures calculated at ambient temperature and pressure.

volume of fuel or oxidant molecules, T_b stands for the adiabatic combustion temperature, S_L is the planar flame velocity, Le represents the Lewis number of hydrogen, $\delta_T = D_T/S_L$ is the thermal thickness of the flame with $D_T = 2.4 \times 10^{-5}$ m/s^2, and $Fr^2 = S_L^2/(gh)$ is the squared Froude number. Values not reported in [14] were calculated using Cantera and PREMIX (Chemkin II) codes.

3. Experimental results

A variety of experimental conditions are described below to provide detailed information on the behavior of lean premixed hydrogen flames, related to the onset and damping of thermoacoustic instabilities. Particularly, the composition of the mixture and the thickness of the channel are known to play decisive roles in hydrocarbon fuels. However, an extensive exploration of hydrogen-air mixtures is unavailable until now and, at first sight, different

considerations to classical studies may apply. Also, the influence of gravity on the flame dynamics is addressed.

3.1. Effect of the mixture composition

To begin with, the effect of the equivalence ratio ϕ is evaluated by keeping a constant 10-mm gap size h for downward-propagating flames. For mixtures with an equivalence ratio lower than the critical value, $\phi \leq \phi_c = 0.36$, the flame experiences strong oscillations due to the coupling with the acoustic waves present in the chamber. These oscillations can be compared to those found by Veiga-Lopez et al. [1] and Martinez-Ruiz et al. [2] for rich (lean) enough propane and DME (methane) mixtures propagating in a similar geometry.

The left panel of Fig. 2(a) shows the temporal evolution of the flame velocity U_L of an hydrogen-air flame with equivalence ratio $\phi = 0.26$. The instantaneous flame velocity U_L was calculated as $U_L = (Wh)^{-1} dV_b/dt$, considering a flat flame with the same burned volume V_b. Note that, because of a limitation in the visualization region, a discontinuous signal was obtained from consecutive experiments. Fig. 2(b)-left represents the over-pressure within the combustion chamber, upholding the coupling between flame and acoustics that is confirmed later by observing the matching between the Fourier spectra of both the pressure and velocity signals depicted in Fig. 2(c)-left. In this case, the over-pressure rises up to 3 kPa producing an oscillating flame with velocity amplitude of around ± 4 m/s. Moreover,

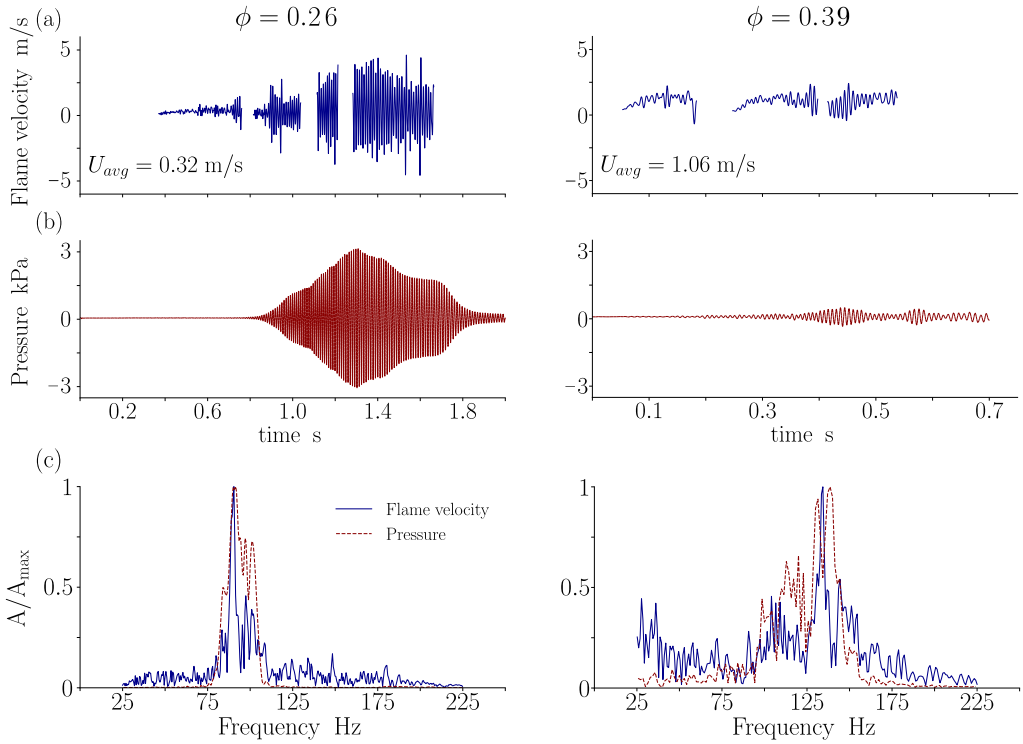

Figure 2: (a) Evolution of the flame velocity with time, for leaner (left) and richer (right) conditions than $\phi_c = 0.36$. The error on the calculation of the velocity is around $\pm 2\%$. (b) Over-pressure signal at the interior of the chamber. (c) Fourier spectra of both signals normalized with the maximum amplitude. The maximum error for these calculations is ± 3 Hz

the phase between both signals, found to be around 1 ms with an error or ± 1 ms due to the limited fps of the high-speed camera, is kept almost constant during the whole propagation of the observed flames. Additionally, we added in Fig. 3-left the Fourier spectrogram of the recorded pressure signal for a $\phi = 0.26$ flame, which analyze the variation of the power level recorded at each frequency with time. The peak is always situated around 100 Hz, increasing with time when the flame is located within the first half of the combustion chamber, but showing a slight decrease once propagating along

the last half of the vessel. The latter could be related to the different dissipation mechanisms present in a real configuration (e.g., viscosity, heat, etc.). Also, the second and third longitudinal modes of the chamber appear in the frequency analysis, but showing a much lower contribution than the first acoustic mode.

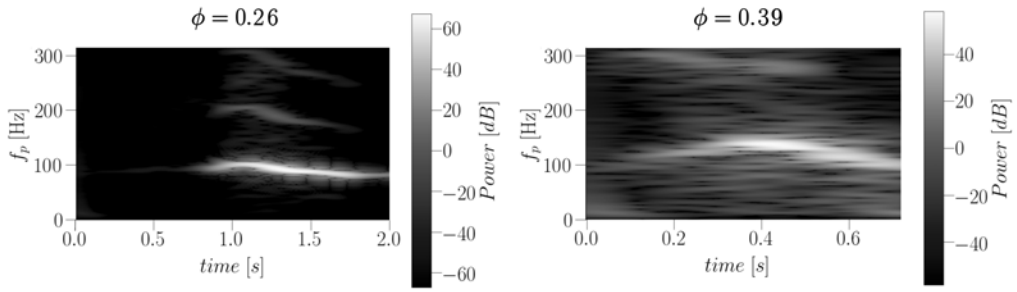

Figure 3: Fourier spectrograms of the pressure signals (f_p) recorded for a hydrogen flame under the secondary ($\phi = 0.26$) and primary ($\phi = 0.39$) regime. The power level at each frequency and time of the signals is calculated by $P = 20 \log_{10}\left(\mathscr{A}/\bar{\mathscr{A}}\right)$ [dB], being $\mathscr{A}$ an instantaneous amplitude and $\bar{\mathscr{A}}$ the average amplitude.

Fig. 4(a)-(f) shows characteristic snapshots of the transition to secondary acoustic instability for a mixture with equivalence ratio $\phi = 0.26$. Once ignited, Fig. 4(a) shows how the flame soon rumples due to hydrodynamic and thermodiffusive instabilities. At this point, the characteristic wavelength of the cells is $\lambda_{\phi=0.26} \sim 6$ mm. Further down Fig. 4(b), some of the frequencies of the ignition noise ($f \approx 85 - 105$ Hz -mixture dependent-) are amplified by the presence of the reactive front, undergoing a feedback mechanism between each other. Here, the flame becomes nearly planar, propagating with an average velocity five times faster than the correspondent laminar burn-

ing velocity S_L and experiencing small-amplitude oscillation at the acoustic frequency. Shortly after, in Fig. 4(c), the pressure waves are further magnified triggering the transition to the secondary instability regime that is identified by the formation of small wrinkles on the quasi-planar flame front with a characteristic wavelength $\lambda_{\phi=0.26} \sim 6.5$ mm. As it is illustrated in Figs. 4(d-e), under the effect of such high-amplitude pressure waves, the reactive front evolves to form flame cells with a longer characteristic wavelength $\lambda_{\phi=0.26} \sim 25$ mm separated by funnels penetrating towards the region occupied by the hot products (d). The pressure-driven flame oscillates at the acoustic frequency with peak flow velocities of around $|U_L| \sim 4$ m/s, one order of magnitude higher than S_L. During the next stage of propagation (e), the flame-cell tips will evolve to form the long funnels, doubling the oscillation period at these particular points (mid-points of the cells and funnels). Nevertheless, the oscillation frequency of the average reaction front position $x_L = \int_0^t U_L dt$ matches the frequency imposed by the pressure waves, as stated by Markstein [10] and Searby [11]. Finally, in Fig. 4(f), the amplitude of the movement is reduced as well as the size of the wrinkles during the final approach to the end of the chamber.

However, for richer H_2-air mixtures ($\phi > \phi_c = 0.36$), only primary acoustic oscillations are observed. The right panels of Fig. 2(a)-(c) show the characteristic velocity observed in a flame with $\phi = 0.39$, the over-pressure within the chamber and the normalized Fourier spectra of the signals respectively. Again, Fig. 3-right depicts the spectogram of the pressure signal. In this

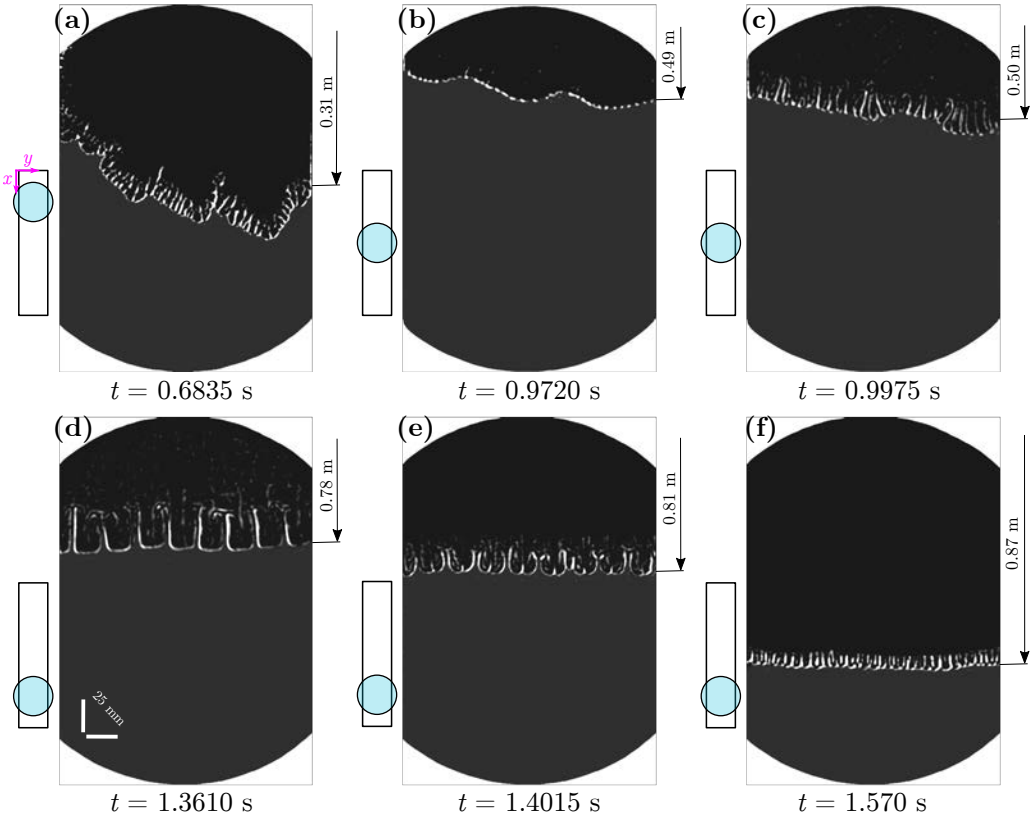

Figure 4: Shadow images of a flame propagating downwards in the primary acoustic oscillatory regime ($\phi = 0.39 > \phi_c$) at different times.

case, the signal is noisier but, still, the first acoustic longitudinal mode at the given conditions of the experiment (i.e., average temperature, chamber geometry, etc.) is found. A similar behaviour of the frequency peak as for the secondary acoustic regime is reported here. Furthermore, Figs. 5(a)-(c) were taken from experiments of flames propagating downwards under the effect of the primary acoustic instability only. Right after ignition (a), the flame shows a similar petal-like shape to that of the previous case. At approximately the

half of the combustion chamber (b), the front experiences small-amplitude ($|U_L| \approx 0.5$ m/s) oscillations with a frequency of $f \approx 135$ Hz. The flame front becomes mostly planar by the effect of weak flame interaction with pressure waves, propagating with a similar outline until it reaches the end wall of the combustion chamber (c). Further enrichment of the mixture introduces other effects that produce different instabilities which are out of the scope of this work. Then, thermoacoustic processes begin to be less important, becoming even negligible.

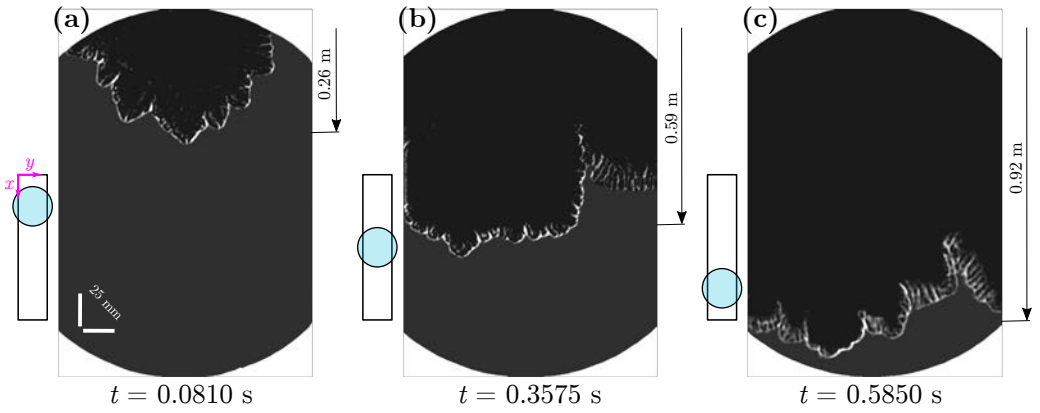

Figure 5: Shadow images of a flame propagating downwards in the primary acoustic oscillatory regime ($\phi = 0.39 > \phi_c$) at different times.

Keeping a constant channel geometry ($h = 10$ mm), the transition to the secondary acoustic oscillations for hydrogen-air premixed flames takes place at $\phi < \phi_c = 0.36$. As already anticipated in [1], this behavior cannot be related neither to laminar burning velocity nor adiabatic flame temperature, as it takes place at very lean mixtures and these parameters show a non-monotonic trend over equivalence ratio. Stronger oscillations would be

expected for $\phi = 0.39$ than for $\phi = 0.26$, finding exactly the opposite behavior. Several works [1, 13, 14, 17, 18], followed the same idea of proposing the Markstein number as the controlling parameter for the transition to instability under consideration of parametric acoustic instabilities. This idea has been applied for various fuels, such as methane, propane and dymethil ether (DME). In consonance with their findings, the transition to the secondary mode would appear for mixtures with a decreasing value of the stabilizing parameter. A similar trend is reported for very lean hydrogen-air mixtures.

3.2. Effect of the channel gap

The geometry of the vessel is known to partly influence the main natural acoustic frequencies that might be excited during the propagation of a flame. Mostly, the length L would determine, given a constant temperature, the main longitudinal acoustic modes at which the front would vibrate. In our experiments, the transverse modes were never reported and therefore we consider that the width W has a second order contribution. This hypothesis is reinforced by the results given in [14], where a vessel of half the width compared to ours shows very similar thermoacoustic behaviour as our thickest channel (i.e., $h = 10$ mm). In this section, we analyze the unchecked influence of the gap size h on the flames propagation by changing the hollow frame thickness from 10 to 4 mm with a 2-mm step for different mixtures. Figure 6 shows, (a) the variation of the maximum over-pressure and (b) the peak frequency of the waves over equivalence ratio for different h. The shad-

owed areas of Fig. 6(a) represent the primary thermoacoustic regions in the pressure-ϕ parametric space. Following similar criteria to those of [1], we consider that a flame experiences secondary acoustic oscillations when simultaneously the over-pressure peak exceeds 1 kPa, the flame position shows a sudden slope change and there are important modifications in the overall outline of the front.

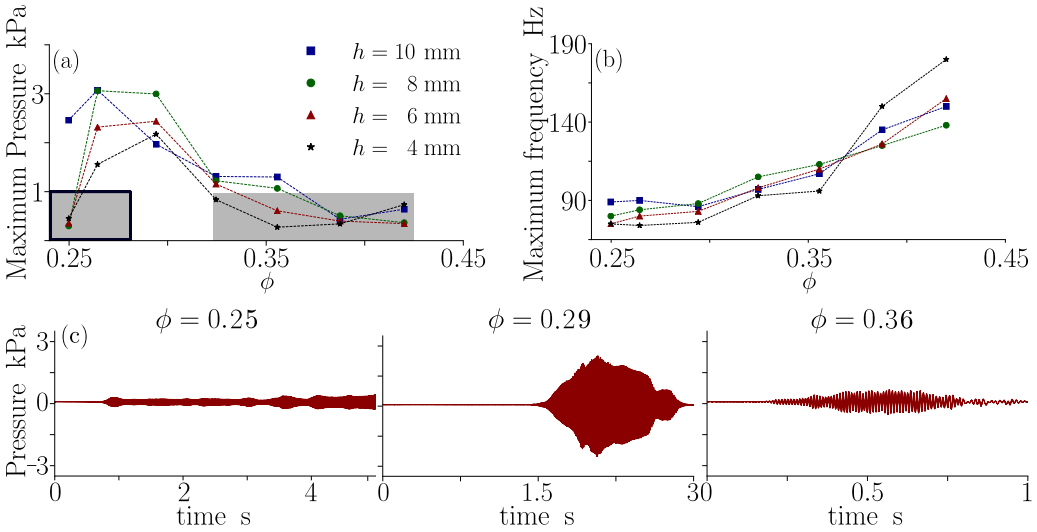

Figure 6: (a) Variation with ϕ of the maximum acoustic pressure in the channel for varying width $h \pm 1\%$. Shadowed areas represent the regions of primary acoustic instability regime. (b) Effect of ϕ on the maximum oscillation frequency for different $h \pm 1\%$. The frequency peaks were found to have an average dispersion of around 0.8% (with a maximum of 2%) . (c) Over-pressure signals obtained in the interior of a $h = 6$ mm chamber for different ϕ.

Modifying the channel thickness h leads to two main changes in the experiments. First, the surface-to-volume ratio increases for decreasing h. This amplifies the conduction heat losses to the surrounding solid walls from both the reaction region and the hot combustion products. Also, thinner channels

lead to the increment of viscous dissipation of the acoustic waves. The acoustic dissipation rate in a channel can be estimated by means of $\sim \mu(v^2/h^2)$, with μ the viscosity of the mixture and v the induced velocity of the flow. For thin enough channels, the characteristic acoustic and viscous dissipation times are comparable [1], thus preventing the arising of acoustic instabilities by channel over-pressure reduction when decreasing h. Furthermore, the peak frequencies of the oscillations slightly reduce due to the diminished flame temperature, directly related to the speed of sound $c = \sqrt{\gamma R_g T}$. Momentum dissipation affects the upper transition limits to the secondary acoustic oscillations, modifying the critical equivalence ratio from $\phi_c \approx 0.36$ ($h = 10$ mm) to $\phi_c \approx 0.32$ ($h = 4$ mm). Also, it should be noted from Fig. 6(a) and (c) that for mixtures of $\phi \leq 0.25$, channels with $h \leq 8$ mm yield major attenuation of pressure waves recovering primary acoustic oscillations.

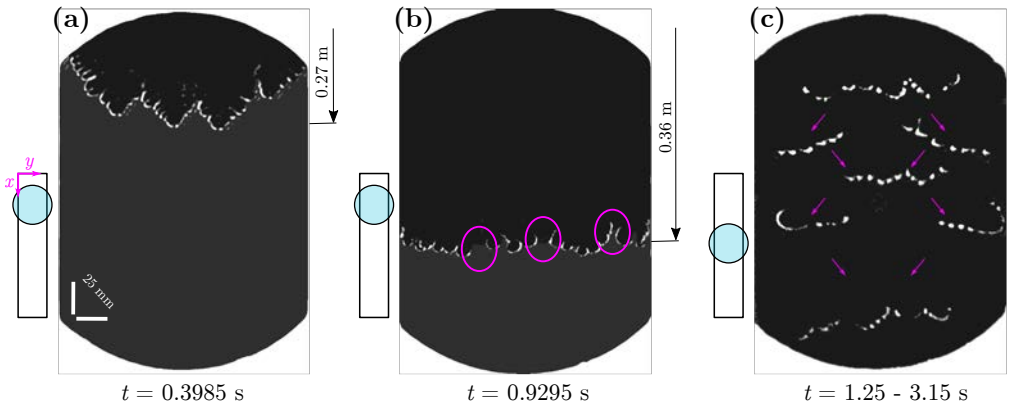

Figure 7: (a)-(c) Post-processed shadow images of a flame propagating downwards in the attenuated primary acoustic oscillations regime for $\phi = 0.25$ and $h = 4$ mm. The circles indicate the partially-quenched areas.

Fig. 7 shows three characteristic images in the evolution of a near-limit flame $\phi = 0.25$ propagating in a 4-mm gap. As explained above for thicker channels or sufficiently rich mixtures, it first oscillates smoothly at the sound frequency without modifying its general outline (a), dominated by hydrodynamic and thermodiffusive instabilities. Later, characteristic quenched areas appear along the front as marked in (b). In fact, heat losses are found to be critical close to the lean flammability limit, being responsible for breaking the front into several parts. Further down the broken front keeps dividing along its propagation (c), zigzagging until it reaches the end of the combustion chamber. This discontinuity of the front leaves several open warm-gases corridors for the acoustic waves to traverse the chamber weakly interacting with the flame. The lower density jump across the front produces a softer reflection of the acoustic waves locally. The feedback interaction is not as strong as for a 10-mm channel, where no quenched areas were found for the same mixture. The waves do not exceed 1-kPa pressure peaks and the flames are not able to transit to the secondary acoustic oscillation regime.

3.3. Buoyancy effects

Gravity has a non negligible effect neither on flame propagation nor thermoacoustics. Its influence is generally evaluated by the Froude number $\mathrm{Fr}^2 = S_L^2/gh$, which compares inertial to gravity effects. The impact of the gravity-driven Rayleigh-Taylor instability [21] on the flame-acoustic coupling for the combustion of lean hydrogen-air mixtures is evaluated by

reversing the combustion chamber, thus the flames propagate upwards. The channel gap size is kept constant $h = 10$ mm and we just varied the equivalence ratio to modify the speed and thermal thickness of the flames. Given a constant acceleration g, the dynamics of slow and thick (lean enough) flames is modified by the increasing importance of the buoyant products.

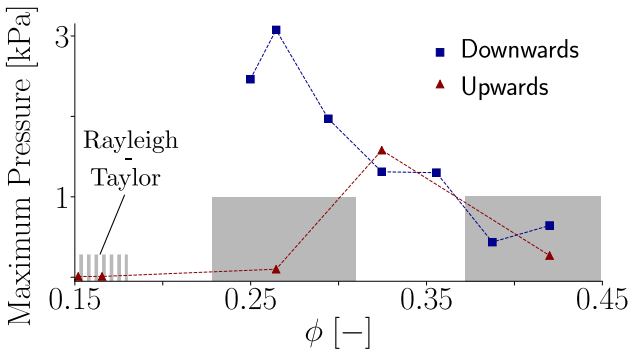

Figure 8: Inner pressure within a $h = 10$ mm Hele-Shaw cell over equivalence ratio ϕ for upward and downward-propagating flames.

The maximum over-pressure within the combustion chamber is plotted in Fig. 8 for both upwards and downwards propagating flames as a function of the equivalence ratio. The flammability limits for upward-propagating flames are extended as a consequence of the gravity-induced flow and of the flame curvature, which enhance flame burning and allows the ignition of leaner mixtures than for downward-propagating flames. Fig. 9 shows representative frames (at $x \sim 0.7$ m from the open ignition end) of flames propagating upwards for the tested mixtures with the corresponding recorded acoustic signals.

From Fig. 8 we know that the effect of gravity is almost negligible for suf-

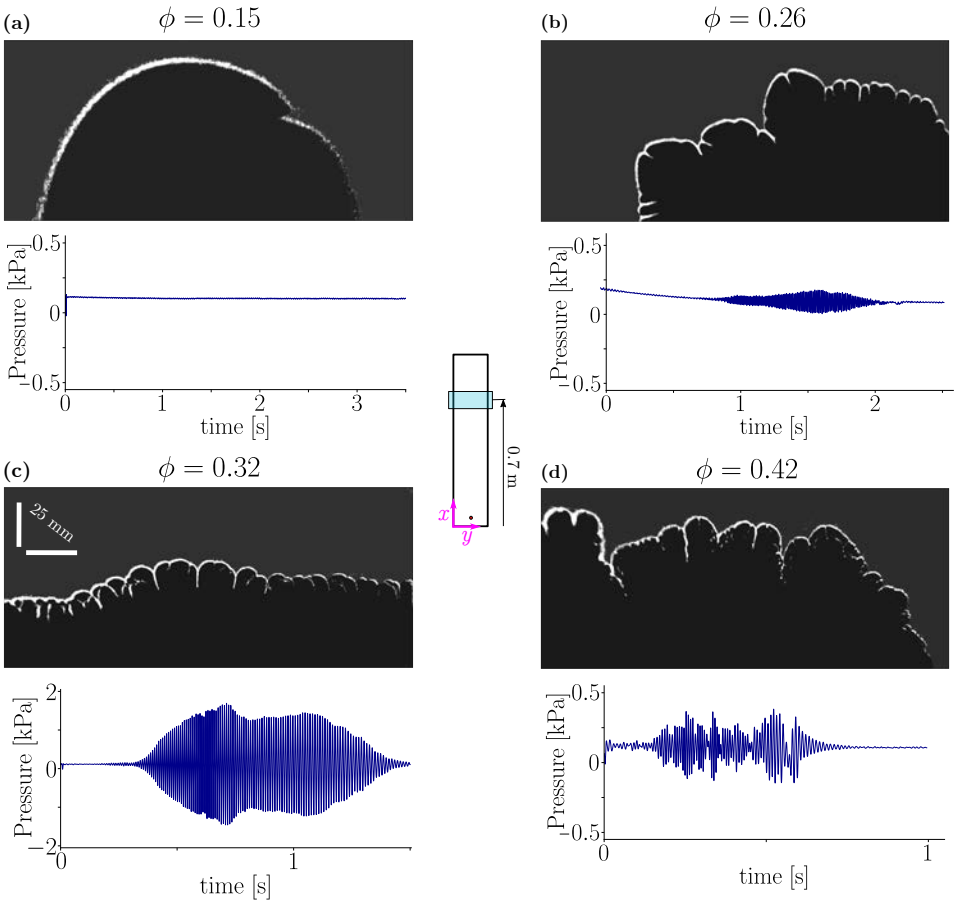

Figure 9: Flame front shapes and recorded over-pressure at the combustion chamber for different hydrogen-air mixtures of upward-propagating flames. The range of acoustic pressure is not kept constant in subfigure (c) to facilitate the reading of the figures.

ficiently fast flames ($\phi \geq 0.32$ and $Fr^2 \geq 0.37$) and the microphones placed inside the combustion chamber only measured slight changes in the acoustic pressure. As an example, we include in Fig. 9(d) the pressure changes measured for a flame with $\phi \geq 0.32$ that propagates in the primary acoustic instability regime. Fig. 9(c) shows a flame leaner than $\phi_c = 0.36$, undergoing secondary oscillations as explained before for downward-propagating flames

with no noticeable changes from gravity effects.

Surprisingly, a new transition from secondary to primary instabilities is identified for leaner mixtures $\phi = 0.26$ in Fig. 9(b), where the flame front remains almost unperturbed by acoustics during its whole propagation. Unlike downward-propagating flames, the change in the maximum acoustic pressures is reduced to a mere 100 Pa. It is clear that gravity ($Fr^2 \leq 0.12$) has an effect on the development of acoustically-driven flame vibrations, eliminating the strong oscillations and favouring the weak primary ones.

We show in Fig. 10 two detail pictures of a $\phi = 0.26$ flame moving towards opposite directions before the acoustics exerts any influence on the propagation of the flame. In Fig. 10(a), the flame propagating downwards presents a wrinkled front with an average wavelength $\bar{\lambda} = 4$ mm that emerge due to hydrodynamic and thermodiffusive instabilities. When moving upwards, gravity modifies the outline of the flame Fig. 10(b) tripling the average wavelength number of the cells formed in the reactive front $\bar{\lambda} = 11$ mm. Linear perturbation analysis [22] anticipates that gravity acting in the opposite direction to that of flame propagation would destabilize the flame for all the possible wave numbers, thus we would expect smaller lobes in upward than in downward-propagating flames. However, hot combustion products rely below fresh heavy reactants, generating an additional upward motion of light products due to buoyancy. Likewise, the curvature of the flame tip induces a flow tangential to the reactive front that convects large wavenumber perturbations from the channel center towards the lateral channel walls [23],

318 stretching the flame and forcing the smooth reactive front observed in the
319 pictures despite of the overall destabilizing effect introduced by gravity.

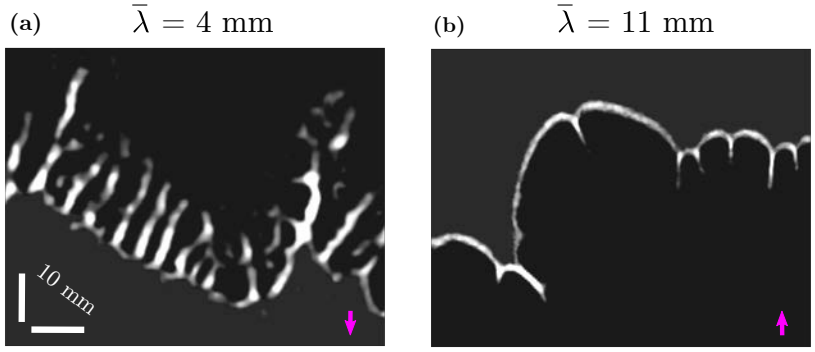

Figure 10: Front detail of two $\phi = 0.26$ flames. The magenta arrows on the bottom corner of the images define the propagation direction. Additionally, the mean wavelength ($\bar{\lambda}$) of each flame front wrinkles is written on top of its correspondent picture.

320 From these observations, we propose the flame shape, characterized by
321 the average wrinkling of the front, as an additional parameter controlling
322 the response of the flame to acoustics perturbations: as the reactive front
323 becomes smoother, the flame becomes more stable regarding thermoacoustic
324 instabilities. To further check this hypothesis, we tested very lean mixtures
325 ($\phi = 0.15$) dominated by buoyancy $Fr \to 0$ in Fig. 9(a). Here, the front
326 is very smooth and acquires the characteristic bubble shape delineated by
327 Rayleigh-Taylor instability, as shown by Levy [24] for other fuels. The size of
328 the bubble flame is of the order of magnitude of the channel width $\bar{\lambda} \sim W =\sim$
329 200 mm, with all the smaller unstable cells convected away by the induced
330 tangential flow [23]. As shown in Fig. 9(a), the pressure recorded within the
331 chamber is constant, evidencing zero feedback between the bubble-like flame

and the pressure waves. In slightly richer mixtures ($\phi = 0.17$), not shown in the figure, a double-headed flame of similar characteristics is observed, again, with no flame-acoustic interaction.

3.4. Discussion

Although it is still not well understood how the flame structure affects the self-induced transition between regimes, a direct relation between front wrinkling and a stronger feedback between acoustic waves and the flame has been reported here. Markstein [25] proposed that local changes of the instantaneous burning velocity and temperature can be directly related to the local curvature of the flame front, defined through the later-named Markstein number $\mathscr{M}$. Therefore, a phenomenological relation of flame speed S_f was provided in the form

$$S_f = S_L - \mathscr{L}\mathscr{K}, \tag{1}$$

where $\mathscr{L}$ represents the Markstein length and $\mathscr{K}$ comprises the flame stretch effects of curvature, strain and flame-surface. Numerous researchers followed this idea [26–34], further developing the theoretical definition of such a concept through linear perturbation analysis in the large activation energy limit. In this limit, the dimensionless activation energy $\beta = E_a(T_b - T_a)/(RT_b^2)$, or Zeldovich number, is assumed to be very large $\beta \to \infty$, reducing the reaction region to a thin surface that can be treated as a discontinuity. In addition, the assumption of nearly-equidiffusional mixtures $\ell = \beta(Le-1) = O(1)$ is required to ensure deviations of the flame temperature from the adiabatic flame

temperature T_b of order β^{-1} and validate the thin-layer approach. This double limit yields an expliticit theoretical expression for the Markstein number

$$\mathscr{M} = \frac{\mathscr{L}}{\delta_T} = \frac{1}{\gamma} \ln \frac{1}{1-\gamma} + \frac{\beta(Le-1)}{2} \left(\frac{1-\gamma}{\gamma} \right) \int_0^{\gamma/1-\gamma} \frac{\ln(1+x)}{x} dx, \qquad (2)$$

where $\gamma = (\rho_u - \rho_b)/\rho_b$ is the gas expansion parameter. This mixture-dependent magnitude proved itself very valuable in the study of general stability of flame fronts, leading to a better understanding of Darrieus-Landau and Rayleigh-Taylor instabilities.

Besides these successful studies, the strain-curvature effect described by the Markstein number was also explored in dynamical problems such as the flame-acoustic wave response. In particular, the theoretical models aiming to explain the flame-acoustic coupling followed the parametric instability analysis proposed by Markstein [10, 13, 17, 18]. These analyses of flame response required the integration of Mathieu's equation to depict the resulting stability diagrams [18, 35] in terms of the the pressure amplitudes and wavenumbers k of the perturbation that are unstable. The magnitude and frequency of the imposed acoustic pressure, the Froude number and the Markstein number were identified on Mathieu's equation as the parameters prescribing the response of the flame to a given perturbation [18].

The following step was to relate the forcing-pressure (parametric) instability, to the self-excited acoustic perturbation [19, 20]. As it was recently

reported there, unstable self-induced pressure oscillations were closely related to the parametric instability regimes. However, the interactions between the flame-induced acoustic pressure and the reactive front were discussed to be far more unstable than flames propagating under an imposed pressure field, outcome that recommends caution in the interpretation of the experimental results based on predictions obtained through Mathieu's equation only.

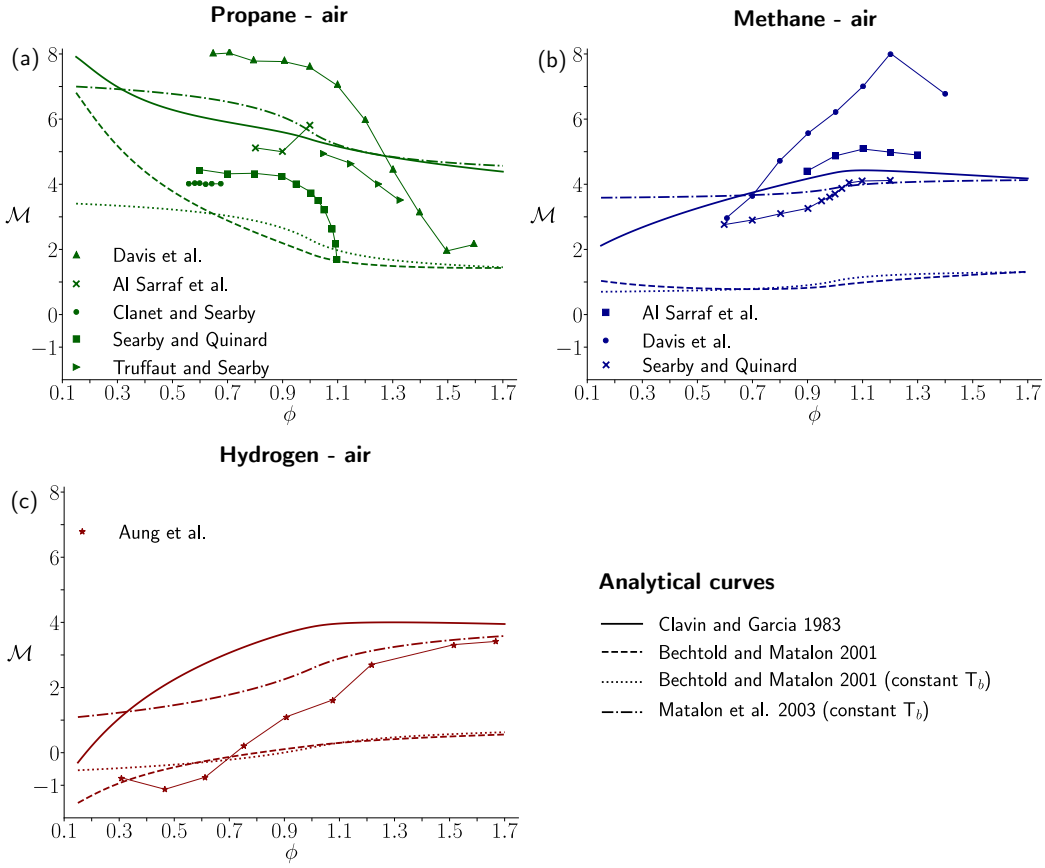

Figure 11: | Compilation of numerical (lines) and experimental (symbols) values of the Markstein number as a function of the equivalence ratio for propane, methane and hydrogen. The experimental values were obtained from [36–41] and the theoretical models taken from [32–34].

For these reasons, the Markstein number variation for different mixtures or equivalence ratios yield modified stability criteria in the theoretical approach, making certain amplitudes and frequencies of acoustic perturbations sufficient to sustain a strong coupling with the flame. This fact reinforces the hypothesis introduced by Aldredge and Killingsworth [13]. Veiga et al [1] identified the thermoacoustic transition below critical values of the Markstein number $\mathscr{M}_c$ based on experimental measurements for methane, propane and DME. Additionally, the numerical calculations carried out by [33, 42] made clear that perturbations of shorter wavelengths are predominant in the front as the Markstein number decreases. This conclusion matches with the classical explanation (see 5.1 in [43]) and with our experimental observations for hydrogen flames, which show that the transition to the secondary oscillatory regime is favored in wrinkled reaction fronts of greater wave number (lower Lewis number).

The dependency of the Markstein number on the equivalence ratio predicted theoretically has been qualitatively confirmed using numerical calculations and experimental measurements for methane, propane and even hydrogen [36–38]. The alarming dispersion between the experimental results provided by different authors, shown in Fig. 11, does not enable a quantitative validation of the theoretical analysis. Furthermore, the classical definition of the Markstein number mentioned above in Eq. 2 assumes nearly-equidiffusive mixtures ($Le \simeq 1$) and large activation energy, what constitutes two primary restriction on the application of this expression to lean

hydrogen flames where diffusive-thermal instabilities and wide reaction regions are found, as was early discussed by Clavin and Williams [29] amongst others. Therefore, the validity of Mathieu's equation and the consequent stability diagrams for flame-acoustic instabilities theoretically rely on flame-sheet model perturbations and a proper definition of $\mathscr{M}$, yet to be clarified for highly-diffusive species with Le significantly below unity, and should not be used to interpret the experimental observations of lean hydrogen flames (e.g. $Le \simeq 0.3$). For the reasons stated above, an extension of the classical stability analysis to mixtures with Lewis number significantly below unity is clearly required to include the effect of non-negligible reaction layer thickness and theoretically validate the experimental observations about the transition between the primary and secondary thermoacoustic oscillations presented here.

4. Conclusions

Thermoacoustic instabilities in narrow channels are studied experimentally for very lean hydrogen-air premixed flames. In particular, the effect of equivalence ratio, channel thickness and gravity on the transition from the primary to the secondary regime is assessed. During the primary acoustic oscillations, the flame remains mostly unperturbed by the pressure waves. It flattens and oscillates at a determined frequency until it reaches the end of the channel. Upon transition, the front experiences violent oscillations related to the high acoustic pressure peaks within the chamber. Additionally,

the outline of the flame changes, presenting a characteristic finger-like shape until reaching the closed end of the chamber, where the waves are attenuated. The transition from primary to secondary acoustic oscillations takes place for hydrogen mixtures leaner than a critical value ϕ_c, geometry dependent.

The Markstein number $\mathscr{M}$ has been discussed to be the best candidate to control the transition between the two described regimes because of its variation with equivalence ratio, decreasing for leaner mixtures. Similar results were found in the experimental observations reported in [1], where methane, propane and dymethilether flames with a smaller average cell size (lower $\mathscr{M}$) were acoustically unstable. This points out the importance of flame stretch on triggering the secondary thermoacoustic instability. These observations appoint the front shape as a possible parameter in the transition between the different instability modes identified in Fig. 4 and 5. Nevertheless, special care must be taken when describing the response of highly-diffusive flames with the available theoretical analyses.

The importance of the combustion chamber thickness is studied by varying h from 10 mm down to 4 mm. Three main modifications are found when reducing this parameter. First, the maximum acoustic pressure reduces for thinner channel as the viscous and heat losses become more important. Second, the transition from the primary to secondary regimes appears at leaner hydrogen-air mixtures. And third, the primary acoustic oscillations are recovered for channels whose thickness is $h \leq 8$ mm for very lean ($\phi = 0.25$) flames. It is related to the increase of energy losses (heat loss and viscous

damping) to the surrounding solid walls, which provoke local extincted areas and break the flames, thus reducing acoustic coupling.

Additionally, for sufficiently lean and slow flames ($\phi \lesssim 0.26$ in our particular configuration), gravity becomes critical regarding thermoacoustics instabilities. Is at this point when the Rayleigh-Taylor instability turns out to be relevant in the description of upward-propagating flames reducing the wrinkling of the reactive front and almost eliminating the flame-acoustics coupling. For ultra lean mixtures, Rayleigh-Taylor dominates the flow and the flame develops a characteristic smooth bubble-shaped. For these kind of flames, thermoacoustic instability is absent. To sum up, lean downward-propagating flames develop a wrinked reaction front with smaller flame cells and they present a greater sensibility to acoustic feedback that rises the acoustic pressure up to 3 kPa. Much less acoustic feedback is found in flames propagating upwards, with bigger average cell size and less flame wrinkling. A direct relation between response to corrugation through related flame stretch processes, characterized here by the Markstein number $\mathscr{M}$, and acoustic coupling was found. Nevertheless, we remark that a direct application of the classical description (2) is not adequate in the theoretical analysis of highly-diffusive lean hydrogen mixtures although the behavior of these flames mimics those of equidiffusive mixtures in terms of acoustic coupling.

5. Acknowledgments

This work was supported by projects ENE2015-65852-C2-1-R (MINECO/ FEDER, UE), BYNV-ua37crdy (Fundación Iberdrola España) and KIT. The authors want to thank the technical support of ProScience GmbH. in the construction and operation of the experimental setup. D. Martnez-Ruiz would like to acknowledge F. Higuera for fruitful discussions.

References

[1] F. Veiga-López, D. Martínez-Ruiz, E. Fernández-Tarrazo, M. Sánchez-Sanz, Experimental analysis of oscillatory premixed flames in a hele-shaw cell propagating towards a closed end, Combustion and Flame 201 (2019) 1–11.

[2] D. Martínez-Ruiz, F. Veiga-López, M. Sánchez-Sanz, Premixed-flame oscillations in narrow channels, Physical Review Fluids 4 (10) (2019) 100503.

[3] R. Aldredge, Methane-air markstein numbers from measurements of thermoacoustic instability, Combustion science and technology 177 (5-6) (2005) 1023–1047.

[4] I. Jain, Hydrogen the fuel for 21st century, International journal of hydrogen energy 34 (17) (2009) 7368–7378.

[5] D. Martínez-Ruiz, F. Veiga-López, D. Fernández-Galisteo, V. N. Kurdyumov, M. Sánchez-Sanz, The role of conductive heat losses on the formation of isolated flame cells in hele-shaw chambers, Combustion and Flame 209 (2019) 187–199.

[6] F. Veiga-López, M. Kuznetsov, D. Martínez-Ruiz, E. Fernández-Tarrazo, J. Grune, M. Sánchez-Sanz, Unexpected propagation of ultra-lean hydrogen flames in narrow gaps, Physical Review Letters (2020) Accepted.

[7] E. Mallard, H. Le Chatelier, Sur les vitesses de propagation de linflammation dans les mélanges gazeux explosifs, Comptes Rendus Hebdomadaires des Séances de lAcadémie des Sciences 93 (1881) 145–148.

[8] W. Mason, R. V. Wheeler, The propagation of flame in mixtures of methane and air. part i. horizontal propagation, Journal of the Chemical Society, Transactions 117 (1920) 36–47.

[9] H. Coward, F. Hartwell, E. Georgeson, Studies in the mechanism of flame movement. part iv. the vibratory period, Journal of the Chemical Society (Resumed) (1937) 1482–1489.

[10] G. H. Markstein, Instability phenomena in combustion waves, in: Symposium (international) on Combustion, Vol. 4, Elsevier, 1953, pp. 44–59.

[11] G. Searby, Acoustic instability in premixed flames, Combustion Science and Technology 81 (4-6) (1992) 221–231.

[12] S. H. Yoon, T. J. Noh, O. Fujita, Onset mechanism of primary acoustic instability in downward-propagating flames, Combustion and Flame 170 (2016) 1–11.

[13] R. C. Aldredge, N. Killingsworth, Experimental evaluation of markstein-number influence on thermoacoustic instability, Combustion and flame 137 (1-2) (2004) 178–197.

[14] J. Yanez, M. Kuznetsov, J. Grune, Flame instability of lean hydrogen–air mixtures in a smooth open-ended vertical channel, Combustion and Flame 162 (7) (2015) 2830–2839.

[15] G. Markstein, Project SQUID. The structure of flames burning in tubes. part 1. flame structure in slow-burning mixtures of hydrocarbons, air and nitrogen, Tech. rep., CORNELL AERONAUTICAL LAB INC BUFFALO NY (1950).

[16] G. Markstein, Interaction of flow pulsations and flame propagation, Journal of the Aeronautical Sciences 18 (6) (1951) 428–429.

[17] G. Markstein, W. Squire, On the stability of a plane flame front in oscillating flow, The Journal of the Acoustical Society of America 27 (3) (1955) 416–424.

[18] G. Searby, D. Rochwerger, A parametric acoustic instability in premixed flames, Journal of Fluid Mechanics 231 (1991) 529–543.

[19] X. Wu, C. K. Law, Flame-acoustic resonance initiated by vortical disturbances, Journal of fluid mechanics 634 (2009) 321–357.

[20] R. C. Assier, X. Wu, Linear and weakly nonlinear instability of a premixed curved flame under the influence of its spontaneous acoustic field, Journal of Fluid Mechanics 758 (2014) 180–220.

[21] Y. Shtemler, G. Sivashinsky, On upward propagating flames, Combustion science and technology 102 (1-6) (1994) 81–93.

[22] P. Clavin, G. Searby, Combustion waves and fronts in flows: flames, shocks, detonations, ablation fronts and explosion of stars, Cambridge University Press, 2016.

[23] A. Zel'Dovich, A. Istratov, N. Kidin, V. Librovich, Flame propagation in tubes: hydrodynamics and stability, Combustion science and technology 24 (1-2) (1980) 1–13.

[24] A. Levy, An optical study of flammability limits, Proceedings of the Royal Society of London. Series A. Mathematical and Physical Sciences 283 (1392) (1965) 134–145.

[25] G. H. Markstein, Experimental and theoretical studies of flame-front stability, Journal of the Aeronautical Sciences 18 (3) (1951) 199–209.

[26] W. Eckhaus, Theory of flame-front stability, Journal of Fluid Mechanics 10 (1) (1961) 80–100.

[27] G. Markstein, Non-steady flame propagation,(1964), AGARDograph, Pergarmon, New York No 75.

[28] P. Clavin, G. Joulin, Premixed flames in large scale and high intensity turbulent flow, Journal de Physique Lettres 44 (1) (1983) 1–12.

[29] P. Clavin, F. Williams, Effects of molecular diffusion and of thermal expansion on the structure and dynamics of premixed flames in turbulent flows of large scale and low intensity, Journal of fluid mechanics 116 (1982) 251–282.

[30] P. Pelce, P. Clavin, Influence of hydrodynamics and diffusion upon the stability limits of laminar premixed flames, Journal of Fluid Mechanics 124 (1982) 219–237.

[31] M. Matalon, B. J. Matkowsky, Flames as gasdynamic discontinuities, Journal of Fluid Mechanics 124 (1982) 239–259.

[32] P. Clavin, P. Garcia, The influence of the temperature dependence of diffusivities on the dynamics, Journal de Mécanique Théorique et Appliquée 2 (2) (1983) 245–263.

[33] J. Bechtold, M. Matalon, The dependence of the markstein length on stoichiometry, Combustion and flame 127 (1-2) (2001) 1906–1913.

[34] M. Matalon, C. Cui, J. Bechtold, Hydrodynamic theory of premixed flames: effects of stoichiometry, variable transport coefficients and arbitrary reaction orders, Journal of fluid mechanics 487 (2003) 179–210.

[35] J. Yáñez, M. Kuznetsov, R. Redlinger, The acoustic–parametric instability for hydrogen–air mixtures, Combustion and Flame 160 (10) (2013) 2009–2016.

[36] K. Aung, M. Hassan, G. Faeth, Markstein numbers and unstretched laminar burning velocities of hydrogen-air flames, in: 33rd Aerospace Sciences Meeting and Exhibit, 1995, p. 374.

[37] S. Davis, J. Quinard, G. Searby, Markstein numbers in counterflow, methane-and propane-air flames: a computational study, Combustion and flame 130 (1-2) (2002) 123–136.

[38] E. Al Sarraf, C. Almarcha, J. Quinard, B. Radisson, B. Denet, P. Garcia-Ybarra, Darrieus–landau instability and markstein numbers of premixed flames in a hele-shaw cell, Proceedings of the Combustion Institute 37 (2) (2019) 1783–1789.

[39] G. Searby, J. Quinard, Direct and indirect measurements of markstein numbers of premixed flames, Combustion and Flame 82 (3-4) (1990) 298–311.

[40] J.-M. Truffaut, G. Searby, Experimental study of the darrieus-landau instability on an inverted-vflame, and measurement of the markstein number, Combustion science and technology 149 (1-6) (1999) 35–52.

[41] C. Clanet, G. Searby, First experimental study of the darrieus-landau instability, Physical review letters 80 (17) (1998) 3867.

[42] A. Patyal, M. Matalon, Nonlinear development of hydrodynamically-unstable flames in three-dimensional laminar flows, Combustion and Flame 195 (2018) 128–139.

[43] P. Clavin, Dynamic behavior of premixed flame fronts in laminar and turbulent flows, Progress in energy and combustion science 11 (1) (1985) 1–59.